CHEMISTRY OF MATERIALS

pubs.acs.org/cm

Article

Atomistic-Scale Simulations of the Graphene Growth on a Silicon Carbide Substrate Using Thermal Decomposition and Chemical Vapor Deposition

Weiwei Zhang and Adri C. T. van Duin*

Cite This: *Chem. Mater.* 2020, 32, 8306–8317

Read Online

ACCESS | Metrics & More | Article Recommendations | Supporting Information

ABSTRACT: Molecular dynamics (MD) studies of graphene growth at the atomistic level can provide valuable insight for understanding its growth mechanism, which is helpful to optimize the growth conditions for synthesizing high-quality, large-scale graphene. In this work, we performed nanosecond timescale MD simulations to explore the graphene growth on a silicon carbide (SiC) substrate with the use of a newly developed ReaxFF reactive force field. On the basis of simulation results at various temperatures from 1000 to 3000 K, we identify the optimal temperature at which the high-quality graphene might be produced. Based on this, we further studied the graphene growth with the silicon thermal decomposition method, and we propose different growth mechanisms on the C-terminated $(00\bar{1})$ and Si-terminated (001) SiC surfaces. We also simulated graphene growth on the Si-facet of SiC substrate using the chemical vapor deposition (CVD) method through sequential C_2H_2 addition, in which the surface catalytic dehydrogenation reactions are included. Furthermore, the temperature effect on catalytic efficiency is discussed. The defect and grain boundary structures of the grown graphene with these two growing strategies are investigated as well. We also provide detailed guidelines on how our atomistic-scale results can assist experimental efforts to synthesize layer-tunable graphene with different growth methods.

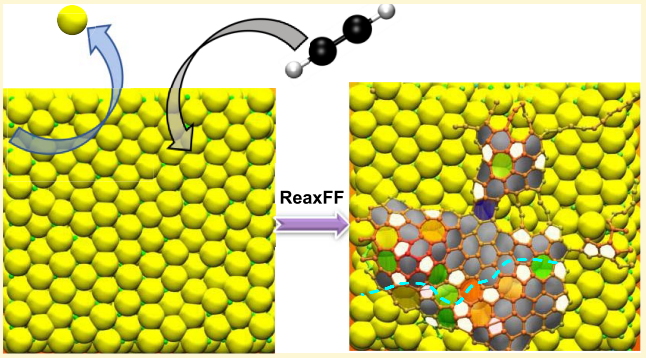

1. INTRODUCTION

Graphene is a unique two-dimensional multifunctional nanomaterial that is composed of sp^2-bonded carbon atoms arranged in a honeycomb lattice. It has been attracted great attention in many fields due to its remarkable mechanical, electronic, optical, thermal, and chemical properties.[1−11] Since it was first isolated from pyrolytic graphite in 2004,[1] various synthetic techniques have been demonstrated to produce high-quality graphene.[12] The most common approaches are the mechanical exfoliation method or the so-called "Scotch tape method,"[1] chemical reduction of graphite oxide,[13,14] high-temperature thermal decomposition of silicon carbide (SiC),[15] chemical vapor deposition (CVD) growth on transition metals (e.g., Cu, Ni, Co, Fe, Pt, Au, etc.) or their alloys (Cu−Ni, etc.), and so on.[16−23] Among these, thermal decomposition of the SiC substrate and CVD on different substrates are the two most widely used methods for the fabrication of high-quality graphene, potentially on a large scale, though both methods possess some general advantages and disadvantages.[24] For instance, it is possible to fabricate devices directly on SiC wafers for the thermal decomposition method, but the SiC crystalline substrate is expensive. The CVD method, on the other hand, is suitable for low-cost and large-scale production, and transfer to other substrates is easy. However, metal catalysts and high temperature are required, and new defects are usually introduced during the transfer process.[25,26]

To improve the quality of grown graphene from thermal decomposition and CVD techniques, many efforts have been devoted to optimizing the experimental conditions, including the growth temperature, pressure and time, the surface orientation of a SiC substrate in the thermal decomposition method,[27] and the carbon source (e.g., methane, acetylene, liquid hexane, etc.[28]), carbon deposition rate, and the substrate materials in the CVD method.[29] For example, the experimental observation shows that excessively low or high temperature usually leads to the deduction of graphene quality;[26] The mechanisms of graphene growth on the Ni and Cu substrates with the CVD method are very different because of their significantly different carbon solubility.[25,30] The Ni-type (i.e., materials with high carbon solubility) graphene growth is governed by the typical segregation mechanism, while the Cu-

Received: May 20, 2020
Revised: September 10, 2020
Published: September 10, 2020

https://dx.doi.org/10.1021/acs.chemmater.0c02121
Chem. Mater. 2020, 32, 8306−8317

type (i.e., materials with low carbon solubility) is classified as surface deposition mechanism.[29]

Due to the complexity of graphene growth, in this work, we are mainly focusing on the two important factors (i.e., the temperature and surface orientation) in control of the quality of graphene growth on a SiC substrate. The SiC substrate is selected on the basis of its two remarkable advantages. One is that graphene is able to grow on various surfaces ((001) or (111)) of different crystal structures (e.g., 6H-SiC, 4H-SiC, 3C-SiC, etc.),[26,31] even though the growth behavior on different surfaces may be significantly different. However, other carbides, such as TiC[32] and TaC,[33] usually need particular crystal structures and even higher temperatures. Another reason is that SiC is an electrically insulating substrate, as such, the grown graphene does not need to be stripped off and transferred for many practical applications.[34] Most recently, an inner and external carbon synergy strategy of graphene growth on a SiC substrate was proposed,[35] which combines the advantages of thermal decomposition and CVD methods and provides an option of fast graphene growth. Therefore, we expect that a theoretical study of graphene growth on a SiC substrate can provide important information and in-depth understanding of the growth process and mechanism in both thermal decomposition and CVD strategies. Accordingly, the atomistic-scale simulations of graphene growth on a SiC substrate have been carried out to reveal the evolution of grown graphene/carbon cluster during the thermal decomposition and CVD treatment, aiming to provide valuable guidance on how to control the growth condition to generate large-scale and high-quality graphene.

Recently, significant theoretical efforts have been dedicated to understand the experimental observation for the graphene substrate on the SiC growth. For example, Tang and Hwang et al. demonstrated that the graphene-like structure appears at temperatures higher than 1300−1500 K based on their simulation results with Tersoff potential.[36,37] Iguchi et al. employed Brenner potential to study the effects of temperature and surface orientation on the quality of graphene.[38] Besides, Nemec et al. tried to reveal the reason of why graphene growth on the C-terminated SiC surface is very different with that on the Si-terminated face with the help of *ab initio* calculations.[39] Most recently, Yu et al. found that the large-scale single-layer graphene formation requires Si sublimation of three SiC bilayers from the *ab initio* molecular dynamics (MD) simulations.[40] A large-scale thermal decomposition simulation was conducted by Takamoto et al. using improved Tersoff potential, which allows us to observe the continuous growth process of the graphene structure with high quality.[41] However, we are noticing that, on the one hand, the *ab initio* methods suffer the drawback of the small size and short time scales. Hence, it cannot display the full picture of the dynamics process of graphene growth. On the other hand, many empirical force fields, such as Tersoff and Brenner, are mainly limited to simulate the thermal decomposition by Si removal. To the best of our knowledge, no proposed empirical potentials are able to study the process of chemical vapor deposition. In addition, although the tight-binding density functional theory (TB-DFT) method, which can be used for relatively large system, has been dedicated to study the graphene and carbon nanotube growth on a variety of substrates, such as Ni, Cu, Fe, SiC, etc.,[42−45] it is still a significant challenge to deal with the system at nanoscale (both spatial and time).[46] To simulate a large-scale system, including the complicated chemical reactions, the ReaxFF reactive force field is a promising tool,[47] since it has been successfully employed to study the growth of many kinds of two-dimensional materials, such as graphene, h-BN, and so on.[48−50]

In this work, we developed a newly Si/H/graphene force field to investigate the graphene growth on a SiC substrate with the framework of ReaxFF reactive MD calculation. To the best of our knowledge, this work studies, for the first time, graphene growth processes by means of both thermal decomposition and CVD strategies on a SiC substrate from the theoretical point of view. Our simulations can provide detailed and direct dynamics information, and it thus may shed light on the central aspects of the growth mechanism of graphene.

2. FORCE FIELD DEVELOPMENT AND COMPUTATIONAL MODELS

2.1. Si/H/Graphene ReaxFF Force Field Parametrization and Validation. The ReaxFF reactive force field developed by van Duin et al.[47] is a bond-order-dependent force field that can describe the bond formation and breaking during the simulation. It determines the connectivity between every pair of atoms using bond-order calculations that is updated at every molecule dynamics time step. The potential can be expressed as[51]

$$E_{\text{system}} = E_{\text{bond}} + E_{\text{angle}} + E_{\text{tors}} + E_{\text{over}} + E_{\text{vdw}} + E_{\text{coul}} + E_{\text{specific}} \quad (1)$$

where E_{bond}, E_{angle}, E_{tors}, and E_{over} are two-body, three-body, four-body energy contributions, and an energy penalty preventing the overcoordination of atoms, respectively. All those terms are bond-order dependent. E_{vdw} and E_{coul} are dispersive and electrostatic contributions between all atoms, regardless of connectivity and bond order. E_{specific} represents specific terms that are not included generally. The details of the ReaxFF potential can be found in the CHO_2008 publication.[52]

The Si/H/graphene ReaxFF force field was developed based on the Si/C/H/O force field parametrized by Newsome et al. in 2012,[53] which does not include an accurate mechanochemical description of graphene. Therefore, we merged carbon parameters of the C-2013 force field[54] in the Si/C/H/O force field training set, to improve the description of the chemistry and dynamics of carbon-condensed phases, such as graphene and fullerenes. In addition, the hydrogen parameters are from the CHO-2016 force field, which shares the same carbon parameters as C-2013 force field but was developed to study a wide range of hydrocarbon chemistry.[55] As such, we expect the new force field is also suitable to study the CVD process. With the newly developed Si/H/graphene force field, the interactions of Si−C, Si−H, Si−Si, C−H, SiC-graphene, etc., can be well described uniformly.

To validate the newly developed force field, we first compared the ReaxFF and DFT bond dissociation energies of Si−C and Si−H bonds, as well as the angle distortion energies for C−C−Si, C−Si−C, Si−C-Si, C-Si−Si, Si−Si−H, C-Si−H, and H-Si−H in select molecules.[56] As shown in Figure S1 in the Supporting Information, the ReaxFF prediction is overall in reasonable agreement with the DFT number. We also considered the equation of state (EOS) for the SiC crystal, which is very important to describe the

https://dx.doi.org/10.1021/acs.chemmater.0c02121
Chem. Mater. 2020, 32, 8306−8317

substrate. As shown in Figure S2, it is found that the ReaxFF prediction of EOS is in good agreement with the DFT calculations. Besides, the ReaxFF predicts a heat of formation for the SiC−diamond phase of 19.95 kcal/mol, which is in good agreement with the DFT number (13.6 kcal/mol).[53] In addition, ReaxFF also gives good prediction for the formation energy of Si adsorbed on graphene, as shown in Table S1, which connects the interaction between a SiC substrate and graphene well. Furthermore, to validate the force field in the description of multimembered carbon rings formation and reconstruction, we compared the results of ReaxFF and DFT for some typical configurations. The DFT calculations were carried out using VASP package.[57] Generalized gradient approximation-Perdew−Burke−Ernzerhof (GGA-PBE) functional and projector augmented wave (PAW) pseudopotentials were used with a cutoff energy of 400 eV in all calculations. The force and SCF energy convergence criteria were set to 0.01 eV/Å and 10^{-5} eV, respectively. Figure S3 shows four typical processes of formation and reconstruction of multimembered carbon rings. For the transformation of five-membered carbon ring to six-membered carbon ring (Figure S3a in the Supporting Information), it is found although ReaxFF underestimates the energy of product from the comparison with DFT number, both ReaxFF and DFT calculations show that this is energetic unfavorable process, due to the four-membered carbon ring formation during this process, and this unstable configuration thus will undergo structure reconstruction quickly. Figure S3b shows the formation process of a seven-membered carbon ring; the reaction energy predicted by ReaxFF is −83.74 kcal/mol, which is in good agreement with that of DFT calculation. The processes of multimembered carbon ring reconstruction (from five- to six-membered carbon ring and defect structure annealing) are shown in Figure S3c,d, respectively. Both reactions are energetically favorable, but they need to overcome reaction barriers in both ReaxFF and DFT calculations. We should mention that although the energy barrier predicted with ReaxFF is lower than that of DFT calculation for each process, it only accelerates the dynamics process of the reconstruction at growth temperature (i.e., the faster graphene growth rate), while it does not change the kinetics too much, due to the much stable product compared to the reactant.

In summary, from the comparison of ReaxFF and DFT results, we conclude that ReaxFF can give a reasonable description of the formation and reconstruction of multimembered carbon rings on a SiC substrate, as well as bond and angle energetics, thus validating the role ReaxFF can play in simulating the graphene growth on the SiC substrate.

2.2. Excess C-Addition Model (ECM). A four-bilayer slab model of the 6H-SiC Si-terminated (001) surface was built to study the temperature effect on the graphene formation. The slab contains four Si-layers with 480 silicon atoms and four C-layers with 480 carbon atoms, respectively. We adopted a 40 Å thick vacuum along the *z*-axis and applied periodic boundary conditions along *x*- and *y*-axes. Subsequently, 200 carbon atoms were randomly placed on the top of the Si-terminated surface by ∼1.8 Å, which is longer than the typical C−C bond length but within the weak interaction scale to hold the added carbon atoms on the surface during the anneal procedure. To get a good sampling, we generated five configurations (ECM-1 to ECM-5). During the MD simulation, the atoms of the bottom bilayer of the slab were fixed to mimic the semi-infinite large surface.[49] Five different annealing temperatures, T = 1000, 1500, 2000, 2500, and 3000 K, were considered here. All of the systems were equilibrated for a total duration of 1.0 ns at the target temperature using the canonical (NVT) ensemble, where number of atoms (N), volume of the simulation box (V), and temperature (T) were kept.

2.3. Thermal Decomposition Model (TDM). Different to the ECM described above, a slab with more bilayers model is necessary to study the thermal decomposition process due to the consumption of Si atoms on the surface during the MD simulation. Here, we built a seven-bilayer slab model of the 6H-SiC surface. As mentioned previously, graphene can be grown on either of the two polar surfaces (C-terminated $(00\bar{1})$ and Si-terminated (001) faces) of the SiC crystal, and both faces show very different mechanism of graphene growth.[12] We thus studied the graphene growth dynamics on both the C-terminated and Si-terminated surfaces. Since the timescale of simulations is only at a nanosecond level while the experiment is usually at hours, it is difficult to capture the Si sublimation behavior in the simulation. Therefore, we studied the graphene growth by gradually and randomly removing the Si atoms during the MD simulation until all of the Si atoms on their top two bilayers are removed completely, rather than removing all the Si atoms in a specific layer at the same time, because the latter one may induce undesirable results, such as the desorption of C atoms and the formation of a 3D-shaped C-cluster.[58] In addition, we investigated the effect of Si removing rate on the graphene growth (Figure S4 in the Supporting Information). It is found that very fast Si removing rate may lead to the system being too far away from equilibrium condition, as a result, the remaining undercoordinated carbon atoms are likely to develop into a three-dimensional amorphous carbon chain. Since we need to balance of effect of Si removing rate on the graphene growth and the computation cost, the Si removing rate was set to 25 ps. Besides, a force-biased Monte Carlo (fbMC) technique[59] was adopted in the TDM simulations, 5000 MC steps every 10 000 MD steps, to accelerate the formation of multimembered carbon rings. Four configurations (TDM-1 to TDM-4) were simulated on each surface at the temperatures of 2000, 2400, and 2800 K. A vacuum slab with 50 Å thick along the *z*-axis and periodic boundary conditions along the *x*- and *y*-axes were also employed.

2.4. CVD Model (CVDM). The CVD model is similar to the TDM described in the previous section, except that the substrate contains five SiC bilayers and the simulated temperatures were set to 2000, 2400, and 2600 K. During the simulation, two C_2H_2 molecules were added at the same time in the vacuum slab with a C_2H_2 adding rate of 25 ps. The distances of the added molecules and the other species (including substrate) are longer than 10 Å so as to guarantee the added molecule to relax sufficiently. Furthermore, to study the defect and grain boundary structures for the grown graphene, we also simulated the system with a high-frequency addition of C_2H_2, i.e., six C_2H_2 molecules were simultaneously added at a temperature of 2400 K. Similarly, we also generated four configurations (CVDM-1 to CVDM-4) and the fbMC technique was adopted in all CVD calculations. Meanwhile, the released H_2 molecule was removed during our simulations.

2.5. Simulation Setup. The current ReaxFF Si/H/graphene force field development was performed with the standalone ReaxFF code, and all MD/fbMC simulations were run with the use of the ReaxFF module of parallel ADF

https://dx.doi.org/10.1021/acs.chemmater.0c02121
Chem. Mater. 2020, 32, 8306−8317

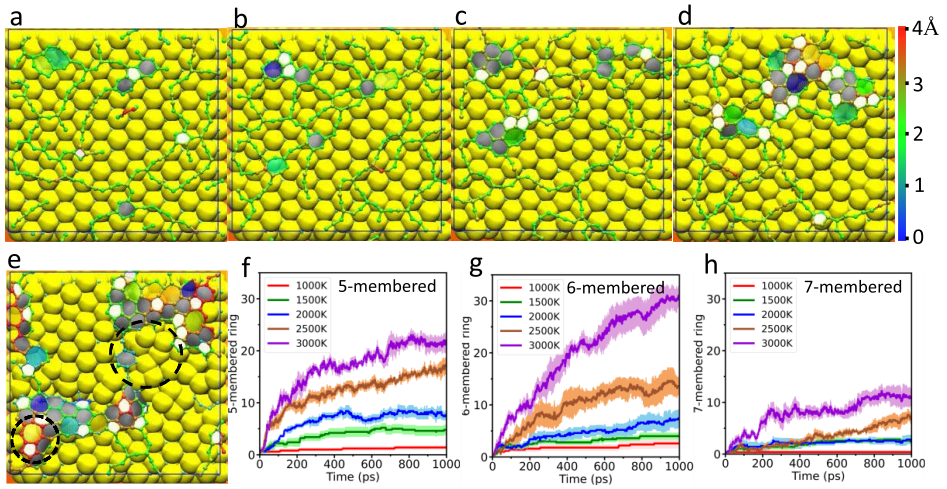

Figure 1. Final snapshots of the graphene growth on the SiC substrate at temperatures of 1000 (a), 1500 (b), 2000 (c), 2500 (d), and 3000 K (e) for configuration ECM-5. The black solid lines show the simulation box. Five-, six-, and seven-membered (including eight-membered) carbon rings are colored by solid white, solid gray, and grid rainbow color, respectively, to highlight their aromatic structures. The Si atoms are shown with yellow spheres, and the red gradient (color bar) of the carbon atoms indicates its distance away from the substrate. (f–h) present the time-dependent numbers of five-, six, and seven-membered carbon rings averaging five ECM configurations at various temperatures. The error bars are shown with the corresponding light color.

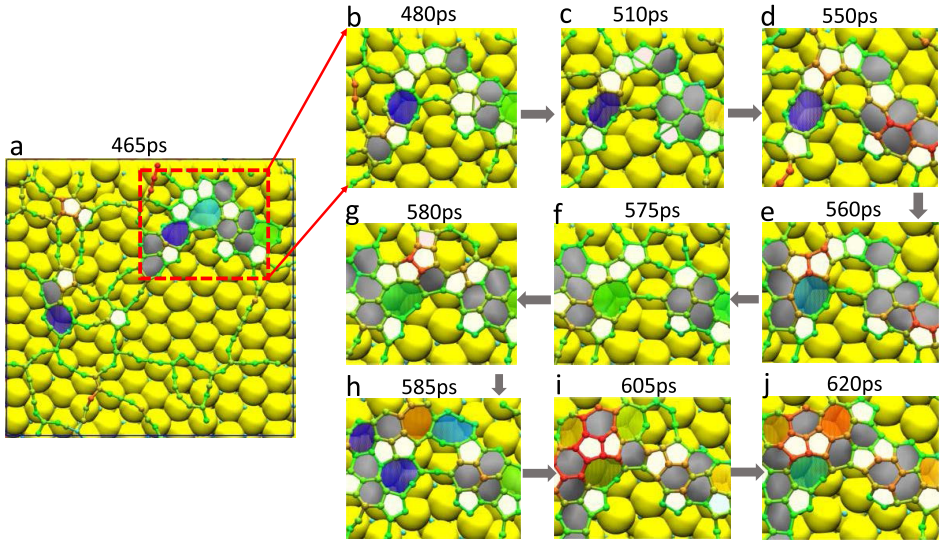

Figure 2. Formation, breakage, and reconstruction processes of multimembered carbon rings for the configuration ECM-5 at the temperature of 2500 K. The color code is the same as that in Figure 1.

package.[60] A velocity Verlet algorithm with a time step of 0.25 fs was employed, and the temperature was maintained by Berendsen thermostat[61] with a damping constant of 100 fs. The presented snapshots were generated using visual molecular dynamics (VMD[62]) or open visualization tool (OVITO[63]).

3. SIMULATION RESULTS AND DISCUSSION

3.1. Temperature Optimization. It is known that temperature plays a key role in the control of the quality of the grown graphene.[12] According to the Arrhenius equation, at higher temperatures, the kinetic energy is able to accelerate the rate of multimembered carbon ring formation. However, too high a temperature may lead to the deformation of the substrate.[30] Therefore, we ran the MD simulations for ECMs in a wide range of temperatures (1000, 1500, 2000, 2500, and 3000 K) to optimize the graphene growth temperature, looking to generate large-scale graphene with high quality. Configuration snapshots of ECM-5 at different temperatures following 1.0 ns simulations are illustrated in Figure 1a–e (other four configurations ECM-1 to ECM-4 are displayed in Figure S5). It shows that at the lower temperatures, such as 1000 K, only a few carbon rings are observed (Figure 1a). With the increase of temperature, more multimembered carbon rings are formed, especially at the temperature as high as 2500 and 3000 K (Figure 1d,e). To quantify the temperature effect on the grown graphene, the numbers of five-, six-, and seven-membered carbon rings as functions of simulation time are compared and shown in Figure 1f–h. It is interesting to see three types of carbon ring formation mechanism with increasing temperature. First, we see a slow diffusion mechanism (i.e., $T < 1000$ K), followed by a fast diffusion-dominated mechanism (i.e., $1000 < T < 2000$ K), and finally a diffusion-reaction-dominated mechanism (i.e., $T > 2000$ K).

https://dx.doi.org/10.1021/acs.chemmater.0c02121
Chem. Mater. 2020, 32, 8306–8317

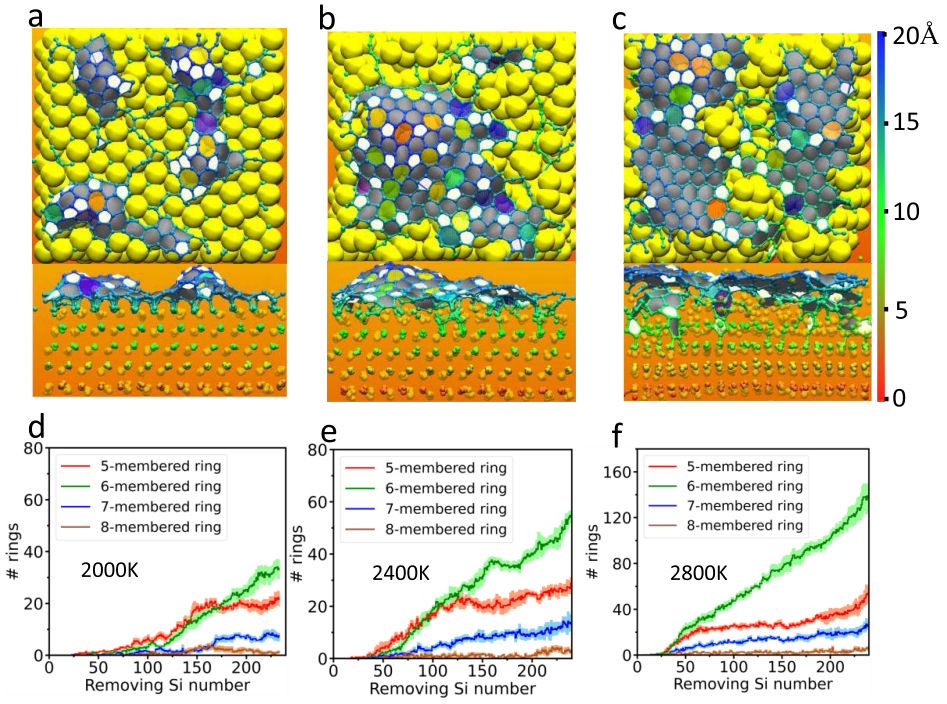

Figure 3. Top and side views of the final snapshots of the configuration TDM-1 are shown in upper panels (a–c), respectively. The Si atoms are shown with yellow spheres, and the blue gradient of the carbon atoms indicates its distance away from the substrate. The color code of the multimembered carbon ring is the same as that in Figure 1. Corresponding numbers of multimembered carbon rings are presented in the lower panels (d–f). The results at temperatures of 2000, 2400, and 2800 K are displayed on the left, middle, and right panels, respectively.

More concretely, when T < 1000 K, the carbon atoms diffuse very slowly due to the relatively strong interaction between a carbon atom and a substrate. Therefore, we observed a slow linear increase of the multimembered carbon ring formation in the simulation time duration. When 1000 < T < 2000 K, the numbers of carbon rings show a logarithmical increase, i.e., a fast growth rate is observed during the initial 400 ps compared to that in the following period at 1500 K. This result demonstrates a higher temperature can assist the carbon atom diffuse to form carbon chains, resulting in carbon branch and creating various two-dimensional structures further. It is worth mentioning that the number of five-membered ring exceeds the six-membered ring in this temperature range; it indicates that the local carbon-poor environment does not favor the six-membered ring formation but support the five-membered carbon ring formation. This observation is consistent with the "pentagon-first" rule, as discussed elsewhere.[42] Once the five-membered carbon ring formed, it is relatively stable. With the temperature increasing further, the amount of six-membered ring will accumulate and exceed five-membered ring, which means that the defects (i.e., five-membered ring here) can be annealed to form a graphene-like structure with the help of fast carbon diffusion and structure reconstruction. However, too high a temperature may cause the substrate reconstruction and drive the carbon rings to move away from the surface, as shown in the top right and bottom left highlighted areas with dashed lines, respectively. In addition, we should mention that even at high temperature, the defect formations, such as five-, seven-, and eight-membered carbon rings, are commonly observed in our graphene growth simulations, as shown in Figure 1d,e. We expect that this result is due to the very short timescale in the MD simulation (ns) compared to that in the experiment (minutes and hours), similar to the previous simulations of graphene growth on the Ni(111) surface.[30]

To better understand the diffusion-reaction-dominated mechanism, we show a typical structure reconstruction process of multimembered carbon rings on the substrate along with time evolution in our MD simulation for the configuration ECM-5 at 2500 K in Figure 2. Between 465 and 550 ps (Figure 2a–d), the two six-membered carbon rings on the left side are opened due to the neighbor carbon chains stretching. After 10 ps equilibration, the carbon chain diffuses to the edge of a defect graphene-like cluster and forms three six-membered carbon rings and one five-membered carbon rings at 560 ps (Figure 2e). With more carbon atoms aggregate in the red dashed region (Figure 2a), a five-membered carbon ring and a six-membered carbon ring are formed adjacent to the three six-membered rings at 575 ps (Figure 2f). During the time of evolution, a four-membered carbon ring is created at 580 ps (Figure 2g), and it merges with a five-membered carbon ring to generate a seven-membered carbon ring (Figure 2h) quickly due to its large ring strain. At 605 and 620 ps (Figure 2i,j), two five-membered and six-membered carbon rings are formed, resulting in a large area graphene growth. From this discussion, we expect that the dynamics of the carbon chain, which has a high diffusion and reactivity, may play an important role in the structure reconstruction of carbon rings. To confirm this, we simulated five ECM configurations at 3000 K by removing the boundary carbon atoms to avoid the box size limitation of our systems. As shown in Figure S6, all of the added carbon atoms effectively diffuse and aggregate to form graphene islands with much higher quality. Our results also demonstrate the importance of the nucleation of the graphene-like cluster in the large area graphene growth.

We should mention that the carbon concentrations are very low in the above ECM models; we also studied the effect of a high carbon concentration on the graphene growth, i.e., 600 carbon atoms were randomly placed on the top of the Si-

https://dx.doi.org/10.1021/acs.chemmater.0c02121
Chem. Mater. 2020, 32, 8306–8317

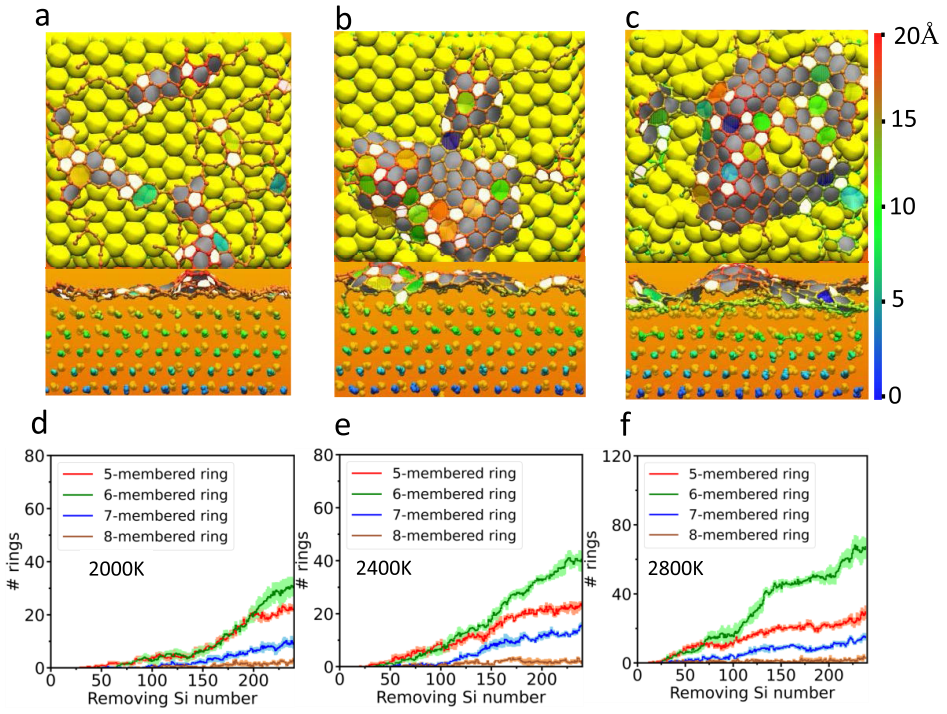

Figure 4. Top and side views of the final snapshots of the configuration TDM-3 are shown in upper panels (a–c), respectively. The Si atom is shown with yellow spheres, and the red gradient of the carbon atoms represents its distance from the substrate. The color code of the multimembered carbon ring is the same as that in Figure 1. The corresponding numbers of multimembered carbon rings are presented in the lower panels (d–f). The results at temperatures of 2000, 2400, and 2800 K are displayed on the left, middle, and right panels, respectively.

terminated. The simulation results are shown in Figure S7 for configurations of ECM-1 to ECM-5. Initially, an amorphous carbon structure in three dimensions is obtained by adding carbon atoms randomly on the surface in a very short simulation period. Because of the excess carbon atoms being added on the top of the surface by a given height, the strongest intensity of the broad peak is located at about 11.0 Å. However, during our simulation, a growing number of multimembered (i.e., 5, 6, and 7) carbon rings is observed (i.e., 500 ps in Figure S7), and the defect graphene structure appears. It is interesting that the broad peak splits two peaks being at 11.0 and 14.3 Å, respectively, and the distance of the two peaks is close to the distance between graphite planes (3.35 Å). With a longer annealing time (i.e., 1.0 ns), it is found the broad peak splits further, indicating the formation of the graphene film with two layers. At the same time, a higher-quality graphene is formed, as shown in Figure S7.

3.2. Thermal Decomposition Simulation. From the discussion of optimal temperature in the previous section, we have a good understanding of the graphene growth mechanism and a general idea of suitable temperature ($2000 < T < 3000$ K), leading to graphene growth with high quality. In this section, we turn to study graphene growth using a thermal decomposition strategy.

Figure 3 displays snapshots for configuration TDM-1 after all Si atoms (240 atoms in total) on top two bilayers were removed from the C-terminated surface (the other three configurations, TDM-2 to TDM-4, are shown in Figure S8 in the Supporting Information). At the low temperature (i.e., 2000 K), with Si-atom removal, some local C-rich regions are created and small size multimembered carbon clusters are formed, and these carbon clusters are likely to bind with the carbon atoms of the SiC crystal surface in the form of C–C bonds, which restricts their dynamics, resulting in the formation of multiple carbon caps, as shown in the side-viewed snapshot at 2000 K (Figure 3a). With increasing temperature, we observe the graphene development gets better, due to the aggregation of graphene-like clusters and more C-atoms separated out from lower SiC bilayers, as shown in the side views of snapshots at 2400 and 2800 K (Figure 3b,c). For example, the SiC surface becomes unstable and triggers reconstruction at around 2400 K, accelerating the carbon clusters dynamics to grow a large area monolayer graphene, as displayed in the top-viewed snapshot (Figure 3b). From Video S1, we observed that the carbon atoms of lower SiC bilayers (rather than just from the Si removal bilayer) also participate in the graphene growth, helping the graphene growth rate due to the carbon-rich environment provided. When the anneal temperature is up to 2800 K, second and further layers of graphene domains appear underneath the preformed graphene sheet, as shown in Figure 3c, indicating that the SiC stability reduces further and more C-atoms are separated out. To better understand the graphene growth at different temperatures, we showed the number of multi-membered carbon rings as a function of Si removal number in Figure 3d–f. It is found at a low temperature (2000 K, shown in Figure 3d), the numbers of five- and six-membered carbon rings are close to each other, which agrees with the conclusion of our temperature optimal simulations, where a local carbon-poor environment favor the formation of five-membered rings. However, the number of six-membered rings becomes larger at 2400 K, as shown in Figure 3e. It indicates that fast thermal dynamics and effective reconstruction of multimembered carbon rings help to improve the quality of grown graphene. At the higher temperature of 2800 K, the amount of six-membered rings is overwhelming that of other multimembered

https://dx.doi.org/10.1021/acs.chemmater.0c02121
Chem. Mater. 2020, 32, 8306–8317

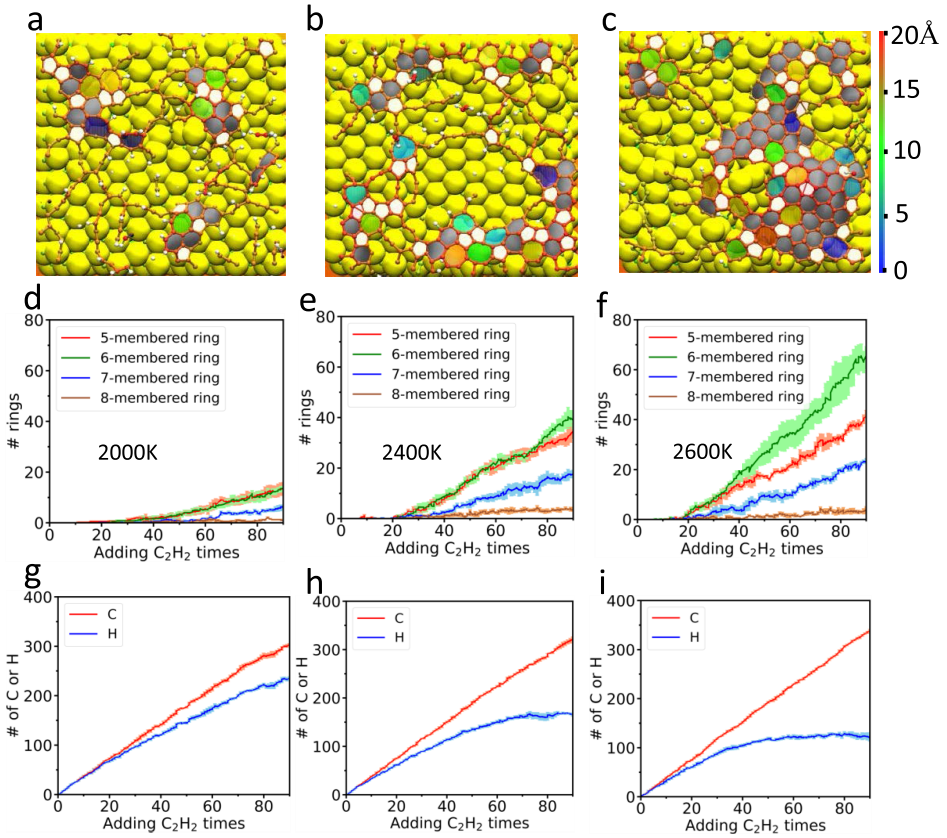

Figure 5. Final snapshots of the configuration CVDM-3 at temperatures of 2000 (left), 2400 (middle), and 2600 K (right) are shown in the upper panels (a–c), respectively. Si and H atoms are shown with yellow and white spheres. The red gradient in the carbon atoms represents their distance from the substrate. The color code for the multimembered carbon rings is the same as that in Figure 1. The corresponding numbers of multimembered carbon rings (d–f) and carbon and hydrogen deposition on the surface (g–i) as the functions of the number of times for the C_2H_2 molecule addition are presented in the middle and lower panels, respectively.

carbon rings, as shown in Figure 3f, which indicates the defects of graphene are annealed further by the high temperature, to produce high-quality graphene. In addition, multilayered graphene is observed due to the carbon atom aggregation in the SiC substrate.

To study the difference of graphene growth on C-terminated with that on Si-terminated SiC substrates, we also simulated the systems with the Si-atom removal from the Si-terminated face. Similar to the TDM simulations on the C-terminated surface, a few carbon clusters are formed at a low temperature of 2000 K, as shown in Figure 4a for configuration TDM-3 (other three configurations TDM-1, TDM-2, and TDM-4 are shown in Figure S9 of the Supporting Information), and the graphene expands with increasing temperature (Figure 4). Differently, we observe the multimembered carbon clusters diffuse more easily on the Si-terminated SiC surface in our simulations, also as indicated from the comparison of their dynamics processes at 2400 K shown in Videos S1 and S2, respectively. This is due to the weaker Si–C bond, compared to the C–C bond. The side-viewed snapshot at 2400 K (Figure 4b) shows that the third top bilayer of the SiC substrate is still stable after all the Si atoms were removed from the first and second top bilayers, which is different with that of the C-terminated surface. During the silicon removal process, we observe from Video S2 that the carbon atoms can freely diffuse to form carbon chains and branches further. With more first-top-bilayer Si atoms removal and fast dynamics, the multi-membered carbon rings are organizing to form a graphene-like structure. Such a structure can also diffuse easily on the SiC surface and undergo structure reconstruction. When the Si atoms in second top bilayer are removed, the remained carbon atoms in this bilayer start to diffuse to the edge of the preformed graphene-like structure and then reconstruct to develop a large-scaled graphene. At the temperature of 2800 K, as shown in Figure 4c, the carbon atoms in the third top bilayer also participate in the graphene growth, but no multilayer graphene is formed. Our simulations demonstrate that the Si-terminated SiC surface is much more stable than the C-terminated surface, which is in good agreement with the *ab initio* theoretical calculations and experimental observations.[39,64]

From our simulations of large-scale graphene growth on the SiC substrate using a thermal decomposition strategy, we have known that the growth mechanisms are different on the C-terminated and Si-terminated surfaces. The analysis of defects and grain boundary for the grown graphene on the two surfaces may be helpful in understanding the defect formation in the experiment. Figures S10 and S11 show the defect and grain boundary on the C-terminated and Si-terminated SiC surfaces at 2400 K with solid and dashed lines, respectively. It is known that Stone–Wales defect (55–77), single vacancy defect (5–9), double vacancy defect (5-8-5 and 555–777), as well as the high-energy inverse Stone–Wales defect (7557), are the well-known defects of graphene in the experiment.[65] In our MD simulations, we can observe 5-8-5, 55–77 defects on the C-terminated surface, and 55–77, 555–777, 5-8-5, and

https://dx.doi.org/10.1021/acs.chemmater.0c02121
Chem. Mater. 2020, 32, 8306–8317

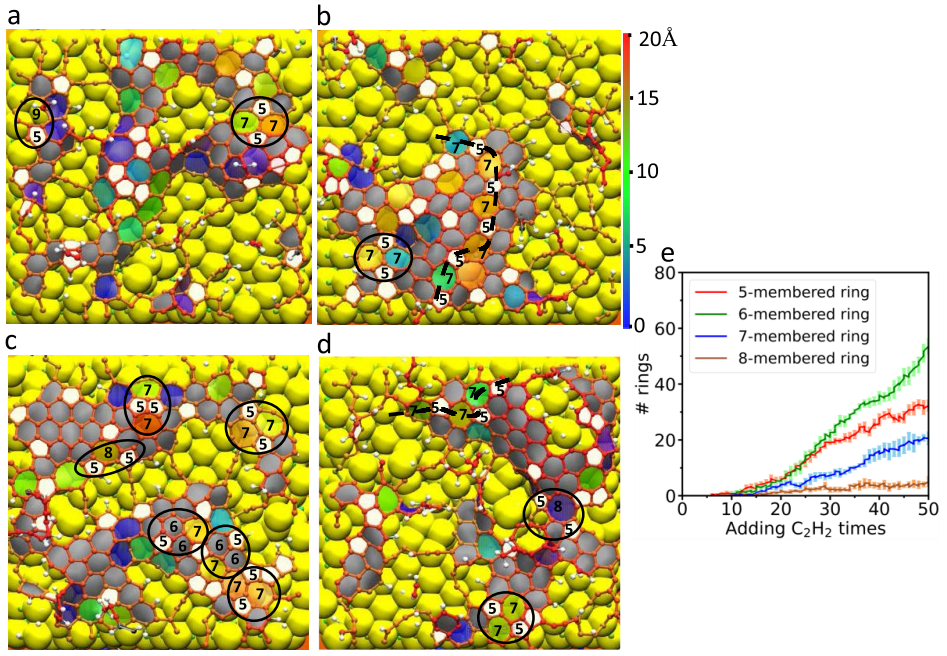

Figure 6. Final snapshots of four CVDM configurations at the temperature of 2400 K (a–d). The defect and grain boundary are shown with solid and dashed lines, respectively. Five-, six-, seven-, and eight-membered carbon rings are colored by solid white, solid gray, and grid rainbow color, respectively, to highlight their aromatic structures. The corresponding numbers of multimembered carbon rings as the functions of the number of C_2H_2 addition events are presented in the lower panels (e).

7557 defects on the Si-terminated surface. Although the concentration of 7557 defect in flat structures can be negligible,[66] this type of defect can be created indeed on the Si-terminated surface under nonequilibrium conditions as shown in the snapshot of configuration TDM-2. Besides, 5-66-7 defects are also observed on both the C-terminated and Si-terminated surfaces. This type of defect may play an important role in the one-dimensional defect (grain boundary) formation.[67] The most common type of grain boundary is 5-7-5-7 type, as shown in configurations of TDM-1 and TDM-2 on the C-terminated surface, and TDM-3 and TDM-4 on the Si-terminated surface. This kind of grain boundary is also very commonly observed in the experiment.[65] To show the dynamics of defects and grain boundary formations, we displayed the snapshots of configurations TDM-1 and TDM-3 on the C-terminated and Si-terminated surfaces in Figures S12 and S13, respectively. It indicates the defect prefers to be generated on the edge of graphene-like structure and the grain boundary is developed through the structure reconstruction of multimembered carbon rings.

In summary, using the ReaxFF MD simulation, we demonstrate that the graphene growth mechanisms through the silicon sublimation method are quite different on the C-terminated and on Si-terminated SiC surfaces due to their different surface stabilities. Our simulations can help us to understand why the experiment shows that the graphene can develop to nine layers on the C-terminated surface while it forms a monolayer on the Si-terminated surface at the annealing temperature about 1250 °C.[64] As graphene growth processes shown in Videos S1 and S2, the carbon atoms in lower SiC bilayers can participate the graphene growth on the C-terminated SiC surface, while it is not the case for the growth on the Si-terminated surface. Namely, the Ni-type growth mechanism,[25] governed by an easy carbon segregation, was observed on the C-terminated SiC surface with a fast growth rate, where the carbon source of graphene comes from both surface and the bulk of the SiC substrate. During this growth process, the structure reconstruction of the SiC substrate may lead to the formation of the multilayer graphene.[68] However, the Si-terminated SiC surface favors a Cu-type growth mechanism at the same temperature,[25] in which the carbon atoms epitaxially diffuse to the edge of preformed graphene-like structure and then undergoes structure reconstruction to form large-scale graphene. Therefore, graphene grows much slower and thinner on the surface, and it is thus more appropriate for the growth of large-scale monolayer graphene.[39,69]

3.3. Chemical Vapor Deposition Simulation. On the basis of the discussion of graphene growth on a SiC substrate through the thermal decomposition strategy, we have found that the Si-terminated surface of SiC is more stable than the C-terminated surface. To reduce the surface effect on the graphene growth during the CVD simulation, we only focus on the graphene growth on the Si-terminated surface using the CVD technique. Figure 5 displays the final snapshots of configuration CVDM-3 (other three configurations CVDM-1, CVDM-2, and CVDM-4 are shown in Figure S14 of the Supporting Information) at temperatures of 2000, 2400, and 2600 K, as well as the average number of multimembered carbon rings, carbon and hydrogen deposition on the surface as the functions of the number of times for C_2H_2 molecules addition. At a temperature of 2000 K, only a few small-sized graphene-like structures are formed and H_2 cannot be released effectively, resulting in high concentrations of H-saturated silicon and carbon atoms (Figure 5a,g), which prohibits the added C_2H_2 molecules from reacting with the SiC surface and the formation of undercoordinated carbon species. When the temperature reaches to 2400 K, large-scale graphene appears. In the same time, the concentrations of H-saturated silicon and carbon atoms are reduced (the number of carbon atoms is

https://dx.doi.org/10.1021/acs.chemmater.0c02121
Chem. Mater. 2020, 32, 8306–8317

significantly greater than the number of hydrogen atoms, as shown in Figure 5h, indicating substantial release of H_2 molecules). It is noted that the presence of hydrogen can saturate the edges of a multimembered carbon ring to keep the graphene-like structure flat (Figure 5b), avoiding the formation of Si−C bonds. Our finding is consistent with the results of *ab initio* calculations for the role of hydrogen in CVD on the Cu(111) surface.[70] From Figure 5e, we find many defects were generated, i.e., the numbers of five-membered rings and six-membered rings are comparable (Figure 5e). Also, significant amounts of the seven-membered rings are formed at present timescale simulation. A further increase of the temperature, such as 2600 K, is helpful to produce higher-quality graphene, but the surface becomes unstable (Figure 5c). Therefore, at this temperature, the graphene might grow from both inner (SiC substrate) and external (C_2H_2) carbon sources, as proposed by Yang et al.[35] In addition, from the comparison of carbon and hydrogen deposition on the surface at different temperatures as shown in Figure 5g−i, we observe that the higher the temperature, the more carbon atoms (but fewer hydrogen atoms) attach to the SiC surface, indicating both hydrogen desorption and dehydrogenation[71,72] can be significantly enhanced. Thus, we expect the high temperature to be helpful for the formation of graphene-like structure in the CVD method. Our results are in good agreement with the experimental observation that graphene develops better with increasing temperature.[73,74] However, as pointed out in the experiment,[75,76] too high temperature might make the substrate unstable, resulting in the uniformity of graphene being not satisfactory and difficult to control its growth.

To study the defects and grain boundary formation during the CVD method, we simulated the system at 2400 K with a high C_2H_2 addition frequency to generate the large-scale graphene. We should mention that a slower carbon flow rate usually leads to a higher-quality graphene for the view of the experiment.[77] However, from the comparison of the results for low- and high-addition frequencies, we did not observe a significant effect on the quality of grown graphene, indicating that the current high-frequency addition is still slow enough to generate high-quality graphene. As shown in Figure 6, we observed 5-9, 55-77, 5-8-5, and 5-66-7 structures, which are well-known defects on the graphene, as well as 7557 defects. Besides, the typical 5-7-5-7 one-dimensional defect is formed, as shown in the configurations CVDM-2 and CVDM-4. This finding is similar to our results for the TDM simulations. From the numbers of multimembered carbon rings, we found more defects are formed at an early stage of CVD simulation, i.e., the number of five-membered ring exceeds that of six-membered carbon ring within 25 times of addition events as shown in Figure 6e; this phenomenon owes to the carbon-poor environment at the early stage of CVD simulations. With more carbon provided, as well as the structure reconstruction, the number of six-membered carbon ring becomes dominant, enhancing the quality of the grown graphene. To show the dynamics of graphene growth, we displayed the number of C_2H_2 addition events dependence of snapshots of configuration CVDM-2 in Video S3. Initially, the C_2H_2 molecule chemical absorbs on the SiC surface and breaks its C−H bond with the help of surface catalysis[71] to form a carbon chain. With more C_2H_2 addition, as well as the carbon chain diffusion, the multimembered carbon rings are then created and developed. A large scale graphene can be generated in the end.

3.4. Discussion of Relevance to the Experiment. From the results of our simulations for the graphene growth using both thermal decomposition and CVD strategies, we expect the size of the grown graphene can be developed as large as the SiC substrate at the optimal temperature, which benefits device processing.[78] The quality of graphene strongly depends on the annealing temperature. Generally, the higher adopted temperature leads to the higher quality (i.e., the honeycomb structure) of graphene. However, too high temperature may cause degradation of the substrate, as a result, the grown graphene will likely lack uniformity and be less controllable. In our simulations, we hypothesized that the rate of Si sublimation from the clean substrate without terraces is the same on both the C-terminated and Si-terminated SiC surfaces. In this condition, we still observed that the graphene growth kinetics undergoes different routes on the Si and C-terminated surfaces, resulting in various growth rates. Namely, the rate of graphene growth on the C-terminated surface is found to be much faster than that on the Si-terminated face, due to their significantly different surface stability.

Based on this, we expect that the monolayer, bilayer, or multilayer graphene growth on different substrate faces can be controlled by specific growth parameters. Since the surface energy of the C-terminated SiC surface is much lower than that of the Si-terminated face, it is thus likely to obtain the multilayer graphene at high temperature, in which the carbon atoms in a bulk substrate are easy to separate out and aggregate to form a multilayer graphene structure. Adopting a low temperature and extended growth time should be helpful in the growth of few layers of graphene, even going down to a monolayer. At lower temperatures, the Si sublimation rate slows down, resulting in a thermodynamic equilibrium or near-equilibrium environment of the surface to avoid carbon atom aggregation from a bulk substrate. In this way, a Ni-type growth mechanism on the C-terminated surface can convert into a Cu-type. Differently, the Si-terminated surface is significantly more stable, and it is feasible to grow a monolayer graphene, where the carbon atoms and graphene-like structure easily diffuse on the surface to develop a large-scale graphene sheet. To grow multilayer graphene, increasing the Si sublimation rate using a higher temperature is an effective way, where the Si-terminated surface becomes far from thermodynamic equilibrium, leading to carbon atom aggregation under the surface. Furthermore, the high temperature can also enhance the reconstruction of multimembered carbon rings to develop high-quality graphene. To control the Si sublimation rate, adjusting the Si background pressure is an alternative, besides the growth temperature, i.e., using a Ar ambient or silicone gas.[78] In addition, our simulations showed that the edge of the graphene is bound to the C-terminated SiC surface with strong C−C bonds, which pushes the graphene far from the surface and forming a cap structure. Therefore, we expect the buffer layer, which is characterized by a carbon-rich interfacial layer covalently binding to the SiC substrate, might be difficult to generate on the C-terminated surfaces. On the contrary, the fast graphene diffusion on the Si-terminated surface indicates a higher opportunity to form a weaker bond between the carbon atoms and Si atoms of the surface, which can benefit the buffer layer formation.

During our CVD simulations, a high temperature is necessary for graphene growth due to the high dehydrogenation energy of C_2H_2 compared to other hydrocarbons,[29] such as the common carbon precursor, CH_4. We expect that the

https://dx.doi.org/10.1021/acs.chemmater.0c02121
Chem. Mater. 2020, 32, 8306−8317

catalytic efficiency of dehydrogenation can be significantly enhanced using the carbon sources with low dehydrogenation energy, resulting in the growth at a lower temperature. For example, by adopting solid and liquid aromatic hydrocarbon, the graphene grows on the Cu substrate at a temperature as low as room temperature.[79] In addition, the low temperature favors the monolayer graphene. On the other hand, the grown graphene at high temperature is more likely to be bilayer or multilayer because carbon atoms are separated out and aggregate from the bulk SiC substrate leading to the formation of more layers underneath the preformed graphene layer. Therefore, it is expected that a layer-tunable graphene can be realized by a combination of the control of temperature and of the carbon sources.

4. CONCLUSIONS

In summary, an overall picture of graphene growth on the silicon carbide (SiC) substrate with thermal decomposition and chemical vapor deposition (CVD) methods was obtained by a systematic study of atomistic-scale molecular dynamics (MD) simulations employing our newly developed Si/H/graphene ReaxFF reactive force field. These simulations show us three types of growth mechanisms: slow diffusion mechanism (at low temperature, i.e., <1000 K), fast diffusion-dominated mechanism (moderate temperature, i.e., 1000 K < T < 2000 K), and diffusion-reaction-dominated mechanism (high temperature, i. e. >2000 K). We found that the low temperature fails to generate large-scale graphene structure, while very high temperatures may destroy the substrate, which against the high-quality monolayer graphene. Based on our results, an optimal growth temperature (~2500 K) is identified for effective graphene growth (i.e., the formation, breakage, and the reconstruction process of multimembered carbon rings in a graphene-like structure). Furthermore, our simulations of the thermal decomposition method study reveal that the graphene grown on the C-terminated SiC surface follows the Ni-type growth mechanism, which is governed by an easy carbon segregation from the surface and bulk of the SiC substrate, while on the Si-terminated surface, it follows a Cu-type growth mechanism at the same temperature, where the surface carbon epitaxially diffuses to the edge of preformed graphene-like structure, due to their different surface stabilities. This observation provides detailed dynamics information that connects well with the common experimental practice that multilayer graphene is usually synthesized on the C-terminated surface, while monolayer graphene is easily generated on the Si-terminated SiC surface. From our CVD simulations, we demonstrate that high temperature is helpful to the formation of a graphene-like structure due to the fast structure reconstruction of multimembered carbon clusters, as well as an enhanced catalytic efficiency for the reaction of the C_2H_2 molecule with the SiC surface, releasing the H_2 molecule or hydrogen transfer to the silicon atoms of the substrate. In addition, we found that the formation of defects and grain boundaries in the grown graphene may be attributable to a local carbon-poor environment and structural reconstruction of the multimembered carbon rings, respectively. These results provide new insights into generating high-quality graphene using both thermal decomposition and CVD techniques. Furthermore, our results indicate that layer-tunable graphene synthesis can be obtained by controlling thermal decomposition/CVD growth temperature and by modifying the carbon CVD source.

■ ASSOCIATED CONTENT

Supporting Information

The Supporting Information is available free of charge at https://pubs.acs.org/doi/10.1021/acs.chemmater.0c02121.

Force field validation; removing rates effect on the graphene growth on the Si-terminated surface; Snapshots for configurations of ECM, TDM, and CVDM; defect and grain boundary for configurations of TDM on both the SiC faces; snapshots and ADFs of ECM models with high carbon concentration; graphene growth processes on both the SiC faces with the thermal decomposition method (PDF)

Graphene growth with the thermal decomposition method at 2400 K on the C-terminated surface of configuration TDM-1 (MP4)

Graphene growth with the thermal decomposition method at 2400 K on the Si-terminated surface of configuration TDM-3 (MP4)

Graphene growth with the chemical vapor deposition method at 2400 K on the Si-terminated surface of configuration CVDM-2 with high-frequency C_2H_2 addition (MP4)

ffield.txt: Si/H/graphene ReaxFF force field parameters (TXT)

■ AUTHOR INFORMATION

Corresponding Author

Adri C. T. van Duin − *Department of Mechanical Engineering, The Pennsylvania State University, University Park, Pennsylvania 16802, United States;* orcid.org/0000-0002-3478-4945; Phone: +1-814-863-6277; Email: acv13@psu.edu

Author

Weiwei Zhang − *Department of Mechanical Engineering, The Pennsylvania State University, University Park, Pennsylvania 16802, United States;* orcid.org/0000-0002-5255-7340

Complete contact information is available at: https://pubs.acs.org/10.1021/acs.chemmater.0c02121

Notes

The authors declare no competing financial interest.

■ ACKNOWLEDGMENTS

This work was conducted with Advanced CyberInfrastructure computational resources provided by The Institute for CyberScience at The Pennsylvania State University (http://ics.psu.edu) and the CyberLAMP cluster, as funded through NSF MRI-1626251. In addition, we used the Extreme Science and Engineering Discovery Environment (XSEDE), which is supported by National Science Foundation grant number ACI-1548562. We also acknowledge funding from NSF-2DCC (NSF MIP/DMR 1539916) and NSF DMR 1808900.

■ REFERENCES

(1) Novoselov, K. S.; Geim, A. K.; Morozov, S. V.; Jiang, D.; Zhang, Y.; Dubonos, S. V.; Grigorieva, I. V.; Firsov, A. A. Electric Field Effect in Atomically Thin Carbon Films. *Science* **2004**, *306*, 666−669.

(2) Novoselov, K. S.; Jiang, Z.; Zhang, Y.; Morozov, S.; Stormer, H. L.; Zeitler, U.; Maan, J.; Boebinger, G.; Kim, P.; Geim, A. K. Room-Temperature Quantum Hall Effect in Graphene. *Science* **2007**, *315*, 1379.

(3) Balandin, A. A.; Ghosh, S.; Bao, W.; Calizo, I.; Teweldebrhan, D.; Miao, F.; Lau, C. N. Superior Thermal Conductivity of Single-Layer Graphene. *Nano Lett.* **2008**, *8*, 902−907.
(4) Bolotin, K. I.; Sikes, K. J.; Jiang, Z.; Klima, M.; Fudenberg, G.; Hone, J.; Kim, P.; Stormer, H. Ultrahigh Electron Mobility in Suspended Graphene. *Solid State Commun.* **2008**, *146*, 351−355.
(5) Lee, C.; Wei, X.; Kysar, J. W.; Hone, J. Measurement of the Elastic Properties and Intrinsic Strength of Monolayer Graphene. *Science* **2008**, *321*, 385−388.
(6) Geim, A. K.; Novoselov, K. S. The Rise of Graphene. In *Nanoscience and Technology: A Collection of Reviews from Nature Journals*; World Scientific, 2010; pp 11−19.
(7) Balandin, A. A. Thermal Properties of Graphene and Nanostructured Carbon Materials. *Nat. Mater.* **2011**, *10*, 569−581.
(8) Lee, J.-H.; Loya, P. E.; Lou, J.; Thomas, E. L. Dynamic Mechanical Behavior of Multilayer Graphene Via Supersonic Projectile Penetration. *Science* **2014**, *346*, 1092−1096.
(9) Yoon, K.; Hwang, G.; Chung, J.; goo Kim, H.; Kwon, O.; Kihm, K. D.; Lee, J. S. Measuring the Thermal Conductivity of Residue-Free Suspended Graphene Bridge Using Null Point Scanning Thermal Microscopy. *Carbon* **2014**, *76*, 77−83.
(10) Achtyl, J. L.; Unocic, R. R.; Xu, L.; Cai, Y.; Raju, M.; Zhang, W.; Sacci, R. L.; Vlassiouk, I. V.; Fulvio, P. F.; Ganesh, P.; et al. Aqueous Proton Transfer across Single-Layer Graphene. *Nat. Commun.* **2015**, *6*, No. 6539.
(11) Yoon, K.; Rahnamoun, A.; Swett, J. L.; Iberi, V.; Cullen, D. A.; Vlassiouk, I. V.; Belianinov, A.; Jesse, S.; Sang, X.; Ovchinnikova, O. S.; et al. Atomistic-Scale Simulations of Defect Formation in Graphene under Noble Gas Ion Irradiation. *ACS Nano* **2016**, *10*, 8376−8384.
(12) Mishra, N.; Boeckl, J.; Motta, N.; Iacopi, F. Graphene Growth on Silicon Carbide: A Review. *Phys. Status Solidi A* **2016**, *213*, 2277−2289.
(13) Stankovich, S.; Dikin, D. A.; Dommett, G. H.; Kohlhaas, K. M.; Zimney, E. J.; Stach, E. A.; Piner, R. D.; Nguyen, S. T.; Ruoff, R. S. Graphene-Based Composite Materials. *Nature* **2006**, *442*, 282−286.
(14) Stankovich, S.; Dikin, D. A.; Piner, R. D.; Kohlhaas, K. A.; Kleinhammes, A.; Jia, Y.; Wu, Y.; Nguyen, S. T.; Ruoff, R. S. Synthesis of Graphene-Based Nanosheets Via Chemical Reduction of Exfoliated Graphite Oxide. *Carbon* **2007**, *45*, 1558−1565.
(15) Berger, C.; Song, Z.; Li, T.; Li, X.; Ogbazghi, A. Y.; Feng, R.; Dai, Z.; Marchenkov, A. N.; Conrad, E. H.; First, P. N.; et al. Ultrathin Epitaxial Graphite: 2d Electron Gas Properties and a Route toward Graphene-Based Nanoelectronics. *J. Phys. Chem. B* **2004**, *108*, 19912−19916.
(16) Niu, T.; Zhou, M.; Zhang, J.; Feng, Y.; Chen, W. Growth Intermediates for CVD Graphene on Cu (111): Carbon Clusters and Defective Graphene. *J. Am. Chem. Soc.* **2013**, *135*, 8409−8414.
(17) Zhang, Y.; Gomez, L.; Ishikawa, F. N.; Madaria, A.; Ryu, K.; Wang, C.; Badmaev, A.; Zhou, C. Comparison of Graphene Growth on Single-Crystalline and Polycrystalline Ni by Chemical Vapor Deposition. *J. Phys. Chem. Lett.* **2010**, *1*, 3101−3107.
(18) Eom, D.; Prezzi, D.; Rim, K. T.; Zhou, H.; Lefenfeld, M.; Xiao, S.; Nuckolls, C.; Hybertsen, M. S.; Heinz, T. F.; Flynn, G. W. Structure and Electronic Properties of Graphene Nanoislands on Co(0001). *Nano Lett.* **2009**, *9*, 2844−2848.
(19) Vinogradov, N. A.; Zakharov, A.; Kocevski, V.; Rusz, J.; Simonov, K.; Eriksson, O.; Mikkelsen, A.; Lundgren, E.; Vinogradov, A.; Mårtensson, N.; et al. Formation and Structure of Graphene Waves on Fe (110). *Phys. Rev. Lett.* **2012**, *109*, No. 026101.
(20) Gao, L.; Ren, W.; Xu, H.; Jin, L.; Wang, Z.; Ma, T.; Ma, L.-P.; Zhang, Z.; Fu, Q.; Peng, L.-M.; et al. Repeated Growth and Bubbling Transfer of Graphene with Millimetre-Size Single-Crystal Grains Using Platinum. *Nat. Commun.* **2012**, *3*, No. 699.
(21) Nie, S.; Bartelt, N. C.; Wofford, J. M.; Dubon, O. D.; McCarty, K. F.; Thürmer, K. Scanning Tunneling Microscopy Study of Graphene on Au(111): Growth Mechanisms and Substrate Interactions. *Phys. Rev. B: Condens. Matter Mater. Phys.* **2012**, *85*, No. 205406.
(22) Wu, Y.; Chou, H.; Ji, H.; Wu, Q.; Chen, S.; Jiang, W.; Hao, Y.; Kang, J.; Ren, Y.; Piner, R. D.; et al. Growth Mechanism and Controlled Synthesis of AB-Stacked Bilayer Graphene on Cu−Ni Alloy Foils. *ACS Nano* **2012**, *6*, 7731−7738.
(23) Ma, W.; Chen, M.-L.; Yin, L.; Liu, Z.; Li, H.; Xu, C.; Xin, X.; Sun, D.-M.; Cheng, H.-M.; Ren, W. Interlayer Epitaxy of Wafer-Scale High-Quality Uniform AB-Stacked Bilayer Graphene Films on Liquid Pt3 Si/Solid Pt. *Nat. Commun.* **2019**, *10*, No. 2809.
(24) Kaur, G.; Kavitha, K.; Lahiri, I. Transfer-Free Graphene Growth on Dielectric Substrates: A Review of the Growth Mechanism. *Crit. Rev. Solid State Mater. Sci.* **2019**, *44*, 157−209.
(25) Ago, H. CVD Growth of High-Quality Single-Layer Graphene. In *Frontiers of Graphene and Carbon Nanotubes*; Springer, 2015; pp 3−20.
(26) Tan, H.; Wang, D.; Guo, Y. Thermal Growth of Graphene: A Review. *Coatings* **2018**, *8*, 40.
(27) Wang, T. *Growth of Epitaxial Graphene on SiC(0001) by Sublimation at Low Argon Pressure*; Université Montpellier, 2018.
(28) Kairi, M. I.; Khavarian, M.; Bakar, S. A.; Vigolo, B.; Mohamed, A. R. Recent Trends in Graphene Materials Synthesized by CVD with Various Carbon Precursors. *J. Mater. Sci.* **2018**, *53*, 851−879.
(29) Yang, X.; Zhang, G.; Prakash, J.; Chen, Z.; Gauthier, M.; Sun, S. Chemical Vapour Deposition of Graphene: Layer Control, the Transfer Process, Characterisation, and Related Applications. *Int. Rev. Phys. Chem.* **2019**, *38*, 149−199.
(30) Xu, Z.; Yan, T.; Liu, G.; Qiao, G.; Ding, F. Large Scale Atomistic Simulation of Single-Layer Graphene Growth on Ni (111) Surface: Molecular Dynamics Simulation Based on a New Generation of Carbon−Metal Potential. *Nanoscale* **2016**, *8*, 921−929.
(31) Chaika, A. N.; Aristov, V. Y.; Molodtsova, O. V. Graphene on Cubic-SiC. *Prog. Mater. Sci.* **2017**, *89*, 1−30.
(32) Terai, M.; Hasegawa, N.; Okusawa, M.; Otani, S.; Oshima, C. Electronic States of Monolayer Micrographite on TiC (111)-Faceted and TiC (410) Surfaces. *Appl. Surf. Sci.* **1998**, *130−132*, 876−882.
(33) Itchkawitz, B.; Lyman, P.; Ownby, G.; Zehner, D. Monolayer Graphite on TaC (111): Electronic Band Structure. *Surf. Sci.* **1994**, *318*, 395−402.
(34) Ouerghi, A.; Silly, M. G.; Marangolo, M.; Mathieu, C.; Eddrief, M.; Picher, M.; Sirotti, F.; El Moussaoui, S.; Belkhou, R. Large-Area and High-Quality Epitaxial Graphene on Off-Axis SiC Wafers. *ACS Nano* **2012**, *6*, 6075−6082.
(35) Yang, Z.; Xu, S.; Zhao, L.; Zhang, J.; Wang, Z.; Chen, X.; Cheng, X.; Yu, F.; Zhao, X. A New Direct Growth Method of Graphene on Si-Face of 6H-SiC by Synergy of the Inner and External Carbon Sources. *Appl. Surf. Sci.* **2018**, *436*, 511−518.
(36) Tang, C.; Meng, L.; Xiao, H.; Zhong, J. Growth of Graphene Structure on 6H-SiC (0001): Molecular Dynamics Simulation. *J. Appl. Phys.* **2008**, *103*, No. 063505.
(37) Hwang, Y.; Lee, E.-K.; Choi, H.; Yun, K.-H.; Lee, M.; Chung, Y.-C. Atomic Behavior of Carbon Atoms on a Si Removed 3C-SiC(111) Surface During the Early Stage of Epitaxial Graphene Growth. *J. Appl. Phys.* **2012**, *111*, No. 104324.
(38) Iguchi, R.; Kawamura, T.; Suzuki, Y.; Inoue, M.; Kangawa, Y.; Kakimoto, K. Molecular Dynamics Simulation of Graphene Growth by Surface Decomposition of 6H-SiC(0001) And. *Jpn. J. Appl. Phys.* **2014**, *53*, No. 065601.
(39) Nemec, L.; Lazarevic, F.; Rinke, P.; Scheffler, M.; Blum, V. Why Graphene Growth Is Very Different on the C Face Than on the Si Face of SiC: Insights from Surface Equilibria and the (3×3)−3C−SiC $(\bar{1}\,\bar{1}\,\bar{1})$ Reconstruction. *Phys. Rev. B: Condens. Matter Mater. Phys.* **2015**, *91*, No. 161408.
(40) Yu, K.; Zhao, W.; Wu, X.; Zhuang, J.; Hu, X.; Zhang, Q.; Sun, J.; Xu, T.; Chai, Y.; Ding, F.; Sun, L. In Situ Atomic-Scale Observation of Monolayer Graphene Growth from SiC. *Nano Res.* **2018**, *11*, 2809−2820.
(41) Takamoto, S.; Yamasaki, T.; Nara, J.; Ohno, T.; Kaneta, C.; Hatano, A.; Izumi, S. Atomistic Mechanism of Graphene Growth on a SiC Substrate: Large-Scale Molecular Dynamics Simulations Based on

https://dx.doi.org/10.1021/acs.chemmater.0c02121
Chem. Mater. 2020, 32, 8306−8317

a New Charge-Transfer Bond-Order Type Potential. *Phys. Rev. B: Condens. Matter Mater. Phys.* **2018**, *97*, No. 125411.
(42) Wang, Y.; Page, A. J.; Nishimoto, Y.; Qian, H.-J.; Morokuma, K.; Irle, S. Template Effect in the Competition between Haeckelite and Graphene Growth on Ni(111): Quantum Chemical Molecular Dynamics Simulations. *J. Am. Chem. Soc.* **2011**, *133*, 18837−18842.
(43) Li, H.-B.; Page, A. J.; Wang, Y.; Irle, S.; Morokuma, K. Sub-Surface Nucleation of Graphene Precursors near a Ni(111) Step-Edge. *Chem. Commun.* **2012**, *48*, 7937−7939.
(44) Page, A. J.; Yamane, H.; Ohta, Y.; Irle, S.; Morokuma, K. QM/MM Simulation of SWNT Nucleation on Transition-Metal Carbide Nanoparticles. *J. Am. Chem. Soc.* **2010**, *132*, 15699−15707.
(45) Ogasawara, N.; Norimatsu, W.; Irle, S.; Kusunoki, M. Growth Mechanisms and Selectivity for Graphene or Carbon Nanotube Formation on SiC($000\bar{1}$): A Density-Functional Tight-Binding Molecular Dynamics Study. *Chem. Phys. Lett.* **2014**, *595*−*596*, 266−271.
(46) Gao, J.; Xu, Z.; Chen, S.; Bharathi, M. S.; Zhang, Y. W. Computational Understanding of the Growth of 2d Materials. *Adv. Theory Simul.* **2018**, *1*, No. 1800085.
(47) van Duin, A. C.; Dasgupta, S.; Lorant, F.; Goddard, W. A. ReaxFF: A Reactive Force Field for Hydrocarbons. *J. Phys. Chem. A* **2001**, *105*, 9396−9409.
(48) Lu, Y.; Yang, X. Molecular Simulation of Graphene Growth by Chemical Deposition on Nickel Using Polycyclic Aromatic Hydrocarbons. *Carbon* **2015**, *81*, 564−573.
(49) Meng, L.; Sun, Q.; Wang, J.; Ding, F. Molecular Dynamics Simulation of Chemical Vapor Deposition Graphene Growth on Ni (111) Surface. *J. Phys. Chem. C* **2012**, *116*, 6097−6102.
(50) Liu, S.; van Duin, A. C.; van Duin, D. M.; Liu, B.; Edgar, J. H. Atomistic Insights into Nucleation and Formation of Hexagonal Boron Nitride on Nickel from First-Principles-Based Reactive Molecular Dynamics Simulations. *ACS Nano* **2017**, *11*, 3585−3596.
(51) Senftle, T. P.; Hong, S.; Islam, M. M.; Kylasa, S. B.; Zheng, Y.; Shin, Y. K.; Junkermeier, C.; Engel-Herbert, R.; Janik, M. J.; Aktulga, H. M.; et al. The ReaxFF Reactive Force-Field: Development, Applications and Future Directions. *npj Comput. Mater.* **2016**, *2*, No. 15011.
(52) Chenoweth, K.; van Duin, A. C.; Goddard, W. A. ReaxFF Reactive Force Field for Molecular Dynamics Simulations of Hydrocarbon Oxidation. *J. Phys. Chem. A* **2008**, *112*, 1040−1053.
(53) Newsome, D. A.; Sengupta, D.; Foroutan, H.; Russo, M. F.; van Duin, A. C. Oxidation of Silicon Carbide by O2 and H2O: A ReaxFF Reactive Molecular Dynamics Study, Part I. *J. Phys. Chem. C* **2012**, *116*, 16111−16121.
(54) Srinivasan, S. G.; van Duin, A. C.; Ganesh, P. Development of a ReaxFF Potential for Carbon Condensed Phases and Its Application to the Thermal Fragmentation of a Large Fullerene. *J. Phys. Chem. A* **2015**, *119*, 571−580.
(55) Ashraf, C.; van Duin, A. C. Extension of the ReaxFF Combustion Force Field toward Syngas Combustion and Initial Oxidation Kinetics. *J. Phys. Chem. A* **2017**, *121*, 1051−1068.
(56) Chenoweth, K.; Cheung, S.; van Duin, A. C.; Goddard, W. A.; Kober, E. M. Simulations on the Thermal Decomposition of a Poly (Dimethylsiloxane) Polymer Using the ReaxFF Reactive Force Field. *J. Am. Chem. Soc.* **2005**, *127*, 7192−7202.
(57) Kresse, G.; Furthmüller, J. Efficiency of ab-Initio Total Energy Calculations for Metals and Semiconductors Using a Plane-Wave Basis Set. *Comput. Mater. Sci.* **1996**, *6*, 15−50.
(58) Morita, M.; Norimatsu, W.; Qian, H.-J.; Irle, S.; Kusunoki, M. Atom-by-Atom Simulations of Graphene Growth by Decomposition of SiC(0001): Impact of the Substrate Steps. *Appl. Phys. Lett.* **2013**, *103*, No. 141602.
(59) Neyts, E. C.; Shibuta, Y.; van Duin, A. C.; Bogaerts, A. Catalyzed Growth of Carbon Nanotube with Definable Chirality by Hybrid Molecular Dynamics − Force Biased Monte Carlo Simulations. *ACS Nano* **2010**, *4*, 6665−6672.
(60) te Velde, G.; Bickelhaupt, F. M.; Baerends, E. J.; Fonseca Guerra, C.; van Gisbergen, S. J.; Snijders, J. G.; Ziegler, T. Chemistry with ADF. *J. Comput. Chem.* **2001**, *22*, 931−967.
(61) Berendsen, H. J. C.; Postma, J. P. M.; van Gunsteren, W. F.; DiNola, A.; Haak, J. R. Molecular Dynamics with Coupling to an External Bath. *J. Chem. Phys.* **1984**, *81*, 3684−3690.
(62) Humphrey, W.; Dalke, A.; Schulten, K. VMD: Visual Molecular Dynamics. *J. Mol. Graphics* **1996**, *14*, 33−38.
(63) Stukowski, A. Visualization and Analysis of Atomistic Simulation Data with OVITO−the Open Visualization Tool. In *Modelling and Simulation in Materials Science and Engineering*; IOP Publishing Ltd., 2009; Vol. *18*, 015012.
(64) Srivastava, N.; He, G.; Feenstra, R. M.; Fisher, P. Comparison of Graphene Formation on C-Face and Si-Face SiC {0001} Surfaces. *Phys. Rev. B: Condens. Matter Mater. Phys.* **2010**, *82*, No. 235406.
(65) Banhart, F.; Kotakoski, J.; Krasheninnikov, A. V. Structural Defects in Graphene. *ACS Nano* **2011**, *5*, 26−41.
(66) Lusk, M. T.; Carr, L. D. Nanoengineering Defect Structures on Graphene. *Phys. Rev. Lett.* **2008**, *100*, No. 175503.
(67) Yazyev, O. V.; Louie, S. G. Topological Defects in Graphene: Dislocations and Grain Boundaries. *Phys. Rev. B: Condens. Matter Mater. Phys.* **2010**, *81*, No. 195420.
(68) Strupinski, W.; Grodecki, K.; Wysmolek, A.; Stepniewski, R.; Szkopek, T.; Gaskell, P.; Gruneis, A.; Haberer, D.; Bozek, R.; Krupka, J.; Baranowski, M. Graphene Epitaxy by Chemical Vapor Deposition on SiC. *Nano Lett.* **2011**, *11*, 1786−1791.
(69) De Heer, W. A.; Berger, C.; Ruan, M.; Sprinkle, M.; Li, X.; Hu, Y.; Zhang, B.; Hankinson, J.; Conrad, E. Large Area and Structured Epitaxial Graphene Produced by Confinement Controlled Sublimation of Silicon Carbide. *Proc. Natl. Acad. Sci. U.S.A.* **2011**, *108*, 16900−16905.
(70) Li, P.; Li, Z.; Yang, J. Dominant Kinetic Pathways of Graphene Growth in Chemical Vapor Deposition: The Role of Hydrogen. *J. Phys. Chem. C* **2017**, *121*, 25949−25955.
(71) Gajewski, G.; Pao, C.-W. Ab Initio Calculations of the Reaction Pathways for Methane Decomposition over the Cu(111) Surface. *J. Chem. Phys.* **2011**, *135*, No. 064707.
(72) Qi, M.; Ren, Z.; Jiao, Y.; Zhou, Y.; Xu, X.; Li, W.; Li, J.; Zheng, X.; Bai, J. Hydrogen Kinetics on Scalable Graphene Growth by Atmospheric Pressure Chemical Vapor Deposition with Acetylene. *J. Phys. Chem. C* **2013**, *117*, 14348−14353.
(73) Cabrero-Vilatela, A.; Weatherup, R. S.; Braeuninger-Weimer, P.; Caneva, S.; Hofmann, S. Towards a General Growth Model for Graphene CVD on Transition Metal Catalysts. *Nanoscale* **2016**, *8*, 2149−2158.
(74) Kumar, P.; Lahiri, I.; Mitra, A. Nickel Mediated Few-Layer Graphene Growth on Glass Substrates by Pulsed Laser Deposition. *Results Phys.* **2019**, *14*, No. 102350.
(75) Dathbun, A.; Chaisitsak, S. In *Effects of Three Parameters on Graphene Synthesis by Chemical Vapor Deposition*, The 8th Annual IEEE International Conference on Nano/Micro Engineered and Molecular Systems, IEEE, 2013; pp 1018−1021.
(76) Liu, Q.; Yu, C.; He, Z.; Gu, G.; Wang, J.; Zhou, C.; Guo, J.; Gao, X.; Feng, Z. Chemical Vapor Deposition Graphene of High Mobility by Gradient Growth Method on an 4H-SiC (0001) Substrate. *Appl. Surf. Sci.* **2018**, *454*, 68−73.
(77) Reina, A.; Jia, X.; Ho, J.; Nezich, D.; Son, H.; Bulovic, V.; Dresselhaus, M. S.; Kong, J. Large Area, Few-Layer Graphene Films on Arbitrary Substrates by Chemical Vapor Deposition. *Nano Lett.* **2009**, *9*, 30−35.
(78) Yazdi, G. R.; Iakimov, T.; Yakimova, R. Epitaxial Graphene on Sic: A Review of Growth and Characterization. *Crystals* **2016**, *6*, 53.
(79) Li, Z.; Wu, P.; Wang, C.; Fan, X.; Zhang, W.; Zhai, X.; Zeng, C.; Li, Z.; Yang, J.; Hou, J. Low-Temperature Growth of Graphene by Chemical Vapor Deposition Using Solid and Liquid Carbon Sources. *ACS Nano* **2011**, *5*, 3385−3390.

https://dx.doi.org/10.1021/acs.chemmater.0c02121
Chem. Mater. 2020, 32, 8306−8317